Characterizing the Thermal Performance of a Flow Through Electronics Module (SEM-E Format) Using a Porous Media Model

L.Tang, K.A. Moores, C. Ramaswamy, Y.Joshi

CALCE Electronic Packaging Research Center
University of Maryland
College Park, MD 20742
(email: yogi@eng.umd.edu)

ABSTRACT

The fluid flow and heat transfer characteristics of a SEM-E electronics cooling module were simulated numerically by representing the internal offset fin structure with a Brinkman-Forchheimer-extended Darcy porous media model. A simplified mockup of the module was constructed and operated through a range of flow rates (0.003 - 0.013 kg/s) and heat loads (100 - 200 W). The experimental set-up provided internal pressure drop data for use in the numerical model as well as discrete temperature measurements for validation of the computational results. The model closely captured the qualitative nature of the flow field and generally displayed good quantitative agreement with the measured temperature profile.

NOMENCLATURE

Variables

C_F	inertial coefficient	T	temperature (K)
Cp	specific heat (J/kg K)	u, v, w	velocity coordinates (m/s)
k	thermal conductivity (W/m^2K)	x, y, z	spatial coordinates (m)
K	permeability (m^2)	U_{ref}	initial inlet velocity (m/s)
L	channel length (m)	V	volume (m^3)
m	mass (kg)	$\vec{V}$	velocity vector (m/s)
P	pressure (Pa)	ρ	density (kg/m^3)
q"	heat flux (w/m^2)	Ψ	convergence criterion
$\dot{q}$	volume heat generation (W)	v_D	Darcy velocity (m/s)
$\dot{Q}$	volumetric flow rate (m^3/s)	μ	dynamic viscosity (m^2/s)
S	cross-sectional area of channel (m^2)	ε	porosity

Subscripts

c	maximum normalized change	m	mass
eff	effective properties	p	porous layer
f	fluid	q	heat

I. INTRODUCTION

Compact heat exchangers are widely used in electronics cooling, particularly in avionics applications. A common configuration employed is the flow through Standard Electronics Module of E format (SEM-E), shown in **Figure 1**. A typical air-cooled SEM-E module dissipates about 40 watts when populated with single-chip carriers. High performance modules with multi-chip carriers may dissipate up to 200 W. The SEM-E modules typically use a variety of compact heat exchanger cores with either air or liquid cooling.

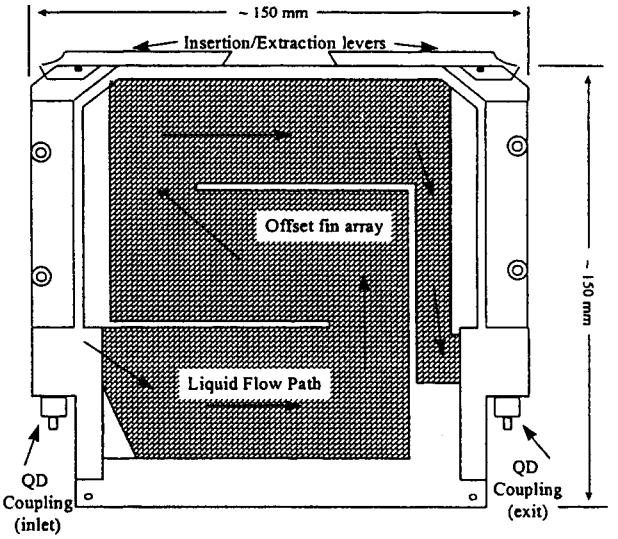

Figure 1: Schematic of typical SEM-E module

The cores contain extended surfaces in a variety of forms (e.g., plain longitudinal fins, offset fins, pin fins, wavy fins etc.). The offset strip fin in particular, has been studied in detail because of its high heat dissipation capacity per unit volume. **Figure 2** shows the basic geometry for rectangular offset fins.

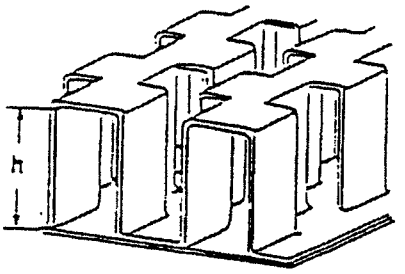

Figure 2: Typical offset fin structure

Early experimental work on characterizing the single phase thermal performance of offset strip fins was carried out by Kays and London [9], who modeled the fin structure as a short, flat plate in laminar flow. Wieting [17], developed empirical correlations for heat transfer and flow friction for a rectangular offset-fin heat exchanger. Suzuki et al. [16] and Xi et al. [18] studied low to middle Reynolds number flow through offset fin structures. Joshi and Webb [7] considered the effects of burred fin ends and roughness of the top and bottom walls of the offset fin arrays. They also developed an empirical model for predicting heat transfer and flow friction both in laminar and turbulent flow. Brinkmann et al. [3] studied the effect of liquid coolants and found a significant enhancement in the heat transfer compared to air cooling. An extensive review of existing correlations for rectangular offset-strip-fin design and modeling , including some of those mentioned above, was made by Manglik and Bergles[11]. They compared a large number of experimental, numerical, and analytical models available in the literature prior to 1990 , and proposed improved design correlations for the heat transfer coefficient and friction factor.

More recently, Hu and Herold [6] found significant effects of Prandtl number in offset fin heat exchanger performance. Flow visualization studies on offset fin heat exchangers have also been reported. Extensive experiments have been performed on actual SEM-E cards at the Naval Surface Warfare Center [4]. Modules with aluminum offset fin cores and silicon carbide (SiC) pin fin cores were tested and the aluminum finned modules were found to show better performance than the SiC pin-fin modules.

There is very little work in the literature however, on numerical modeling of these fin structures. Sparrow and Patankar [14] conducted numerical studies on offset fin structures considering zero fin thickness. Later Patankar and Prakash [13] considered the effect of finite plate thickness. Recently Sridhar [15] modeled the offset fin structure considering a 2-D unit cell to predict heat transfer and pressure drop characteristics. He also considered the effect of 3-D geometry and concluded that except at the inlet and exit, a 2-D model can be fairly accurate in predicting the temperature distribution within the offset fin exchanger core. While these models provide a detailed description of the flow and heat transfer near individual fins, performance analysis of the entire module is impractical due to excessive computing requirements.

The focus of this study is to introduce a new approach to numerically modeling such modules. A typical SEM-E module core is approximately 1.5 mm - 2.5 mm (0.06 in. - 0.10 in.) thick, and the fin structure is quite dense in the core. Such a compact system resembles a porous medium and the well-established equations that govern flow and heat transfer can be extended to describe it. Recently, Antohe et al. [1] have used this approach to model the cold plates in a high frequency microwave system, in which the cold plate core was filled with a porous metal matrix (foam). In this paper, the details of the numerical model are first introduced. The results of the analysis of a SEM-E module configuration are then presented and compared with experimental data.

II. NUMERICAL MODEL

A. *Approach*

Heat transfer in a SEM-E module involves the formation of complex flow and temperature fields around individual fins. At higher velocities, flow separation may occur around the fins, which enhances mixing. While this flow separation leads to a larger pressure drop, the associated mixing substantially enhances the heat transfer rate. Also, the heat

dissipation rate is increased drastically due to the increase in the surface area. Because the fluid saturated fin matrix has a larger effective thermal conductivity than the fluid alone, it augments the heat dissipation from the bounding surface. Since the fluid flows through a tortuous path in a complex fashion, in general, it is not possible to model the flow in full detail. However, the effects of the fin matrix, the local recirculation around the individual fins, and the concomitant thermal dispersion can be incorporated into the conservation equations through a volume averaging process [8].

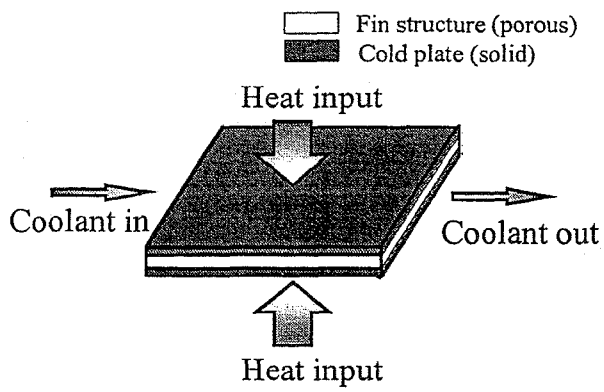

Figure 3: Porous media model of SEM-E module.

The dense offset-strip fin array was approximated as a porous medium in the current study. Traditional porous media analyses utilize Darcian models and neglect non-Darcian effects, such as the viscous shear force along the solid boundaries, and the inertial convective force. For forced convection in a SEM-E module, these non-Darcian effects can be significant. Thus a Brinkman-Forchheimer-extended Darcy model was used in this study. With this model, the Darcian term represents the form drag caused by the presence of the porous medium, the Brinkman term describes the pressure loss caused by viscous shear along the solid boundary, and the Forchheimer term accounts for the pressure drop caused by the local acceleration and separation around the solid particle. The porous medium is considered to be homogeneous and isotropic (**Figure 3**), saturated with fluid, and in local thermodynamic equilibrium with the solid matrix.

B. *Governing Equations*

The flow and heat transfer in the SEM-E module can be described using the following volume averaged continuity, momentum, and energy equations for the finned area. Conventional Navier-Stokes and energy equations are used for the other non-finned area of the module:

Continuity:

$$\frac{\partial u}{\partial x} + \frac{\partial v}{\partial y} + \frac{\partial w}{\partial z} = 0 \qquad (1)$$

Momentum: (for the fin stock)

$$\frac{\rho_f}{\varepsilon^2}(\vec{V} \bullet \nabla\vec{V}) = -\Delta P + \frac{\mu_f}{\varepsilon}\nabla^2\vec{V} - (\frac{\mu_f}{K} + \frac{\rho_f C_F}{\sqrt{K}}|\vec{V}|)\vec{V} \qquad (2)$$

Momentum: (for other parts)

$$\frac{\rho_f}{\varepsilon^2}(\vec{V} \bullet \nabla\vec{V}) = -\Delta P + \frac{\mu_f}{\varepsilon}\nabla^2\vec{V} \qquad (3)$$

Energy: (for fin stock)

$$(\rho C_p)_f(\vec{V} \bullet \nabla T) = k_{eff}\Delta^2 T \qquad (4)$$

Energy: (for other parts)

$$(\rho C_p)_f(\vec{V} \bullet \nabla T) = k_i\Delta^2 T + \dot{q} \qquad (5)$$

where $\dot{q}$ is the volume heat generation rate for the heater, and $\dot{q} = 0$ otherwise.

The averaging method eliminates microscopic phenomena such as local recirculation or dispersion, and thus the equations rely on additional empirical relations for closure. Permeability and form drag coefficient data can be obtained from experimental measurements or geometric relations for the fin structures to provide the needed relations.

Boundary conditions:

The simplified configuration shown in **Figure 4** was used in the numerical modeling (dimensions in mm). Idealized boundary conditions were applied and are summarized as follows:

At z=0, H: q''=0, u=v=w=0
At y=0, W, q''=0, u=v=w=0
At x=0: inlet, $T=T_{ref}$, $u=U_{ref}$, v=w=0;

otherwise, q''=0, u=v=w=0

At x=L: outlet, $\frac{\partial T}{\partial x} = \frac{\partial u}{\partial x} = 0$, v=w=0

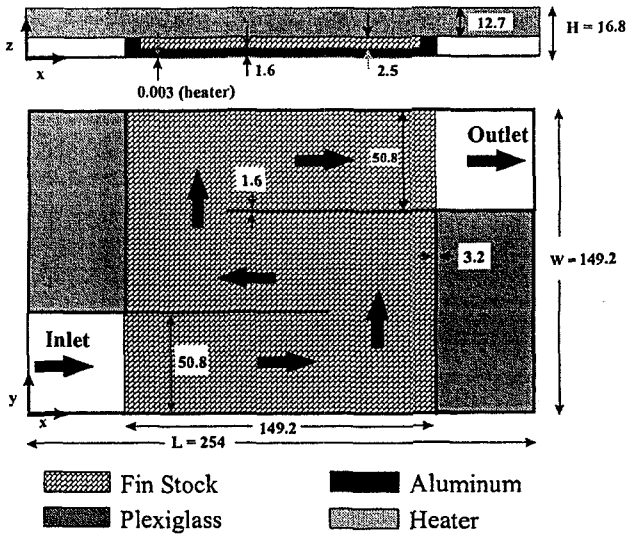

Figure 4: Domain of computation and boundary conditions (all dimensions in mm)

C. *Porosity, Permeability and Drag Coefficient*

The porosity of the porous layer is obtained by the following equation:

$$\varepsilon = 1 - \frac{V_s}{V} \qquad (6)$$

where V_s is the solid phase volume and V the total volume of the porous matrix. A unit cell of the fin stock is considered to measure the percentage of solid volume in it.

The permeability (K) of the offset fin array was estimated using two different approaches. In the first, a quadratic fit between pairs of volumetric flow rate ($\dot{Q}$) and corresponding pressure drop per unit length ($\Delta p/L$) using least squares, gives (K) and the drag coefficient (C_F). The equation for the quadratic fit is as follows [1]:

$$\frac{\Delta p}{L} = \frac{\mu}{K} v_D + \frac{\rho C_F}{K^{1/2}} v_D^2 \qquad (7)$$

The Darcy velocity (v_D) is defined as:

$$v_D = \frac{\dot{Q}}{S} \qquad (8)$$

where $\dot{Q}$ is the volumetric flow rate and S the cross sectional area of the test channel.

The pressure drop in the porous layer is calculated as follows:

$$\Delta p = \Delta p_p - \Delta p_f \qquad (9)$$

where Δp_f is the pressure drop with no porous matrix inside and Δp_p the pressure drop with the porous layer.

A second means of estimating the permeability involves treating the fins as a stack of capillary fissures of given width (B) and porosity (ε) [2]. The permeability is then represented by the geometric relation:

$$K = \frac{\varepsilon B^2}{12} \qquad (10)$$

Effective thermal conductivity in the numerical model depends on the porosity and thermal conductivity of the solid and liquid. Modeling the offset fin as parallel structures with coolant and metal, the effective thermal conductivity is calculated as [8]:

$$k_x = k_y = k_z = (1-\varepsilon)k_{fin} + \varepsilon k_f \qquad (11)$$

D. *Numerical solution procedure*

The governing equations were discretized using a staggered grid, and solved numerically using the control volume based finite-difference method. The discretized governing equation, for any variable ϕ (u, v, w, or T) can be written as:

$$a_p \phi_p = \sum a_{nb} \phi_{nb} + b \qquad (12)$$

where the subscripts *p*, and *nb* referred to the grid point P, and its neighboring points, respectively. The discretized source term was denoted by b. The discretized equation for the momentum conservation also contained a pressure term on the right hand side. These equations were solved using an iterative solution procedure. The SIMPLER methodology [12] was used to handle the velocity and pressure coupling. A power law scheme was used to model the convection and diffusion processes at each node.

The discretized equations were solved iteratively in a line by line fashion, using a Tri-Diagonal Matrix Algorithm (TDMA). During the solution, an under relaxation was used to ensure convergence. For any variable, the value at the end of the *ith* iteration was given as:

$$\phi^i = \phi^{i-1} + \alpha(\phi^i - \phi^{i-1}) \qquad (13)$$

The under relaxation factor (α), varied from 0.8 for u, v, w, and T, to 1.0 for the pressure and pressure correction equations.

For convergence, three criteria were satisfied simultaneously. The first was satisfied, when the maximum normalized change in primitive variables (u, v, w, T) between two successive iterations reduced below respective defined quantities (ψ_c). The criterion was defined as:

$$\left|\frac{\phi^i - \phi^{i-1}}{\phi^i}\right|_{max} < \Psi_c \qquad (14)$$

where ϕ represents the primitive variable and i represents the iteration level. ψ_c was set as $1x10^{-4}$ for u, v, and w, and $1x10^{-5}$ for T.

The second criterion satisfied a mass balance:

$$\left|\frac{m_{in}^i - m_{out}^i}{m_{in}^i}\right|_{max} < \Psi_m \qquad (15)$$

ψ_m was set as 0.02.

The last satisfied an energy balance:

$$\left|\frac{Q_{in}^i - Q_{out}^i}{Q_{gen}^i}\right|_{max} < \Psi_q \qquad (16)$$

ψ_q was set as 0.05.

III. EXPERIMENT

A. *Experimental set-up*

A sketch of the experimental layout is shown in **Figure 5.** The set-up was constructed to measure both differential pressure and temperature at discrete points along the flow path of the offset fin stock, within a SEM-E module type configuration. The pressure drop data were used to calculate the permeability and friction drag factor for the porous media model. Temperature measurements were used for comparison with model predictions.

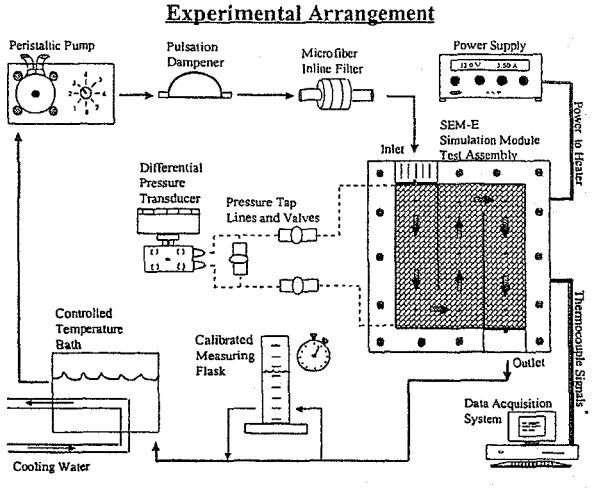

Figure 5: Schematic of experimental set-up for temperature and pressure measurements

A *Masterflex* peristaltic pump controlled the flow in the test loop within a range of $1.67x10^{-6}$ - $25x10^{-6}$ m^3/s (100-1500 ml/min). The liquid pulsation dampener, downstream of the pump, provided a steady flow to the test section, and a micro-fiber filter captured any contaminants larger than 50 μm that might be present in the circulation loop. Flow rates were measured at the outlet of the test section using a precision flask and a stop watch. Water was used as the circulating fluid. The inlet temperature to the test section was maintained within ± 0.5 °C by a *Haake* B3 constant temperature bath[1]. The pressure drop between

[1] While inlet temperature was maintained during testing at a given flow rate, some drift was experienced between different flow rates, especially at higher power dissipation levels, due to the limited cooling capacity of the bath.

the inlet and outlet was determined using an *Omega* PX771 differential pressure transducer, which employs a strain gage and piezo-resistive sensors for pressure measurement. The pulsed current signal from the transducer was converted into a voltage via a precision resistor and measured with a *Fluke* 87 True RMS multimeter. Temperatures were measured using 0.080 mm (3 mil) copper-constantan thermocouples in conjunction with a PC based data acquisition system controlled using Labview.

Details of the test section are illustrated in **Figure 6**. Channels were machined from a single piece of aluminum to construct a three pass heat exchanger plate to act as a SEM-E simulation module. The offset fin array within the channels consisted of (8) individual rectangular sections, situated in series along the channel. Each section was cut at a 45° angle from a single strip of offset fin stock (**Figure 7**) using a diamond saw. Before placing each section into the channel, all four edges were polished smooth with fine grade sand paper to remove any excess material or burrs left by the cutting process. The fin stock dimensions are shown in **Figure 8**.

In an actual SEM-E module, heat dissipated from associated electronics would be transmitted through both top and bottom surfaces to the core structure. In the test set-up used, heat was produced at the bottom surface only. A resistive heating element (12 Ω) was attached to the bottom of the aluminum plate with a thermally conductive epoxy adhesive to provide uniform surface heating to the test section. Power was provided by a pair of *Instek* PR-3060D DC power supplies operated in series. Voltage input was monitored directly at the base of the element's electrical leads with the multimeter. Heater current was indirectly determined by measuring the voltage drop across a network of precision resistors of known resistance. The total heater power was then taken as the product of the measured voltage and calculated current.

The aluminum module, with fin stock, heater, and thermocouples, was enclosed in a 5 piece Plexiglas housing which was sealed with silicone rubber adhesive, and screwed closed. The entire assembly was surrounded by a layer of Styrofoam insulation (25 mm minimum thickness in any direction).

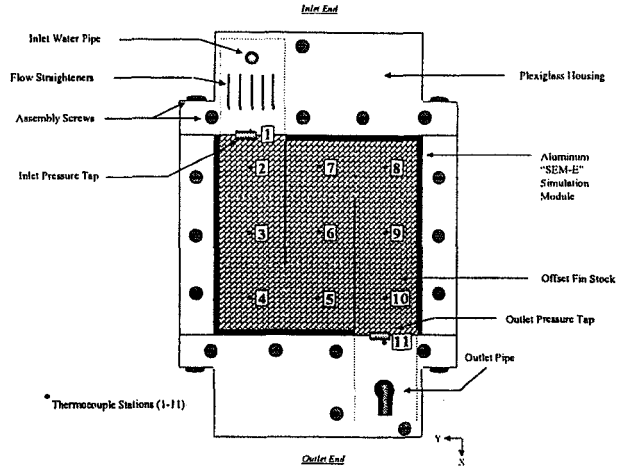

Figure 6: Overhead view of test section

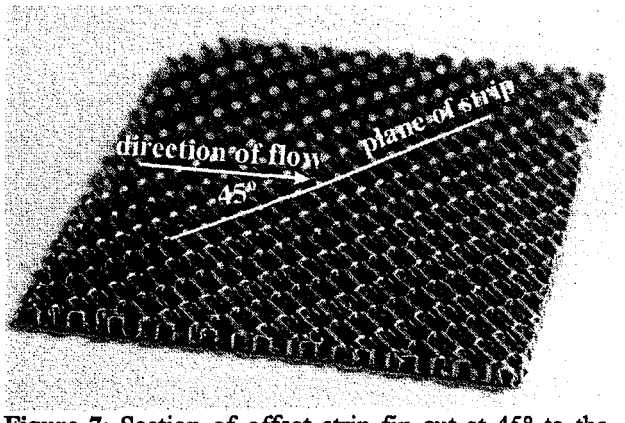

Figure 7: Section of offset strip fin cut at 45° to the plane of the strip.

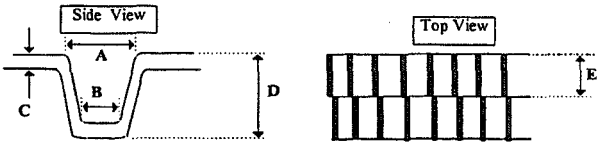

A(mm)	B(mm)	C(mm)	D(mm)	E(mm)
1.48	0.97	0.24	1.27	3.34

Figure 8: Offset fin array dimensions

B. *Experimental Procedure*:

To determine the pressure drop induced by the fins, it was first necessary to measure the drop inherent in the test section alone, with no fin stock in place. Measurements were taken through a range of flows. However, even at the highest flow rate used in these tests, the pressure drop was found to be on the order of only 0.2 kPa (0.03 PsiD). The effect of the test section on pressure drop was therefore neglected in later calculations.

With the fin stock in place, differential pressure was measured between test section inlet and outlet at a series of flow rates ranging from approximately 0.003 to 0.013 kg/s (0.2 - 0.8 l/min). Flow rate was determined with a measuring beaker and stop watch. This was done a minimum of three times, with the average of all samples taken as the representative flow rate. The voltage signal from the pressure transducer was taken once every 100 ms during the flow sampling period and an averaged value was determined by the multimeter. Differential pressures were then calculated using a voltage to pressure conversion equation derived earlier during calibration of the transducer. These ranged from 2.8 to 20.2 kPa over the range of flow rates.

Temperature measurements were taken through a similar range of mass flow rates, with those rates determined in the same manner, and were done separately from the pressure measurement tests. Locations of the thermocouples are shown in **Figure 6.** Temperatures were collected every 2.5 seconds. At each individual flow rate, the test was run until steady state was reached. Temperatures were then collected for an additional 300 seconds (5 minutes), and the averaged values during this period were taken as the representative temperatures for the given flow rate and power level.

Measurement Uncertainties

The uncertainties in the measured quantities were computed using the method of Kline [10] and are summarized in **Table 1.**

Table 1: Estimated measurement uncertainties

Measurement	Uncertainty
Pressure drop	+/- 3.4 %
Mass flow rate	+/- 4.3 %
Temperature	+/- 1.0 %
Power	+/- 1.0 %

IV. RESULTS

From the pressure drop data collected during testing, a permeability (K) of 2.9×10^{-9} m^2 and drag coefficient (C_f) of 0.0188 were calculated using Equation (7). An estimate of K was also made using the geometric relationship described by Equation (10) and was determined to be 8.42×10^{-8} m^2 or roughly an order of magnitude larger than the experimentally derived value.

Initial numerical analyses were made using the experimentally based permeability. However, the numerical model experienced convergence difficulties when applying this value. Further analyses were attempted using the geometrically based value of K and this was found to eliminate the convergence problem. As a result, a parametric study was performed in which K was varied by several orders of magnitude to determine the importance and effect of K on the numerical results.

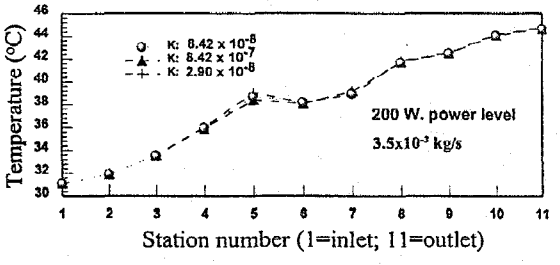

Figure 9: Effect of permeability (K) on calculated temperature profile.

Figure 9 shows results of the study for three values of K for an arbitrarily chosen operating case. The permeabilities shown are for the geometrically based K (8.42×10^{-8} m^2), a permeability one order of magnitude larger than that (8.42×10^{-7} m^2), and K= 2.90×10^{-8} m^2 which is an order of magnitude higher than that found by Equation (7) and approximately the largest value of K which did not create a convergence problem.

It was found that within the given range, the permeability has only a weak influence on the resulting temperature distribution. Therefore all subsequent analyses were made using the geometrically based K (and the experimentally obtained value for C_f).

Velocity and temperature profiles obtained from the numerical model for a power input of

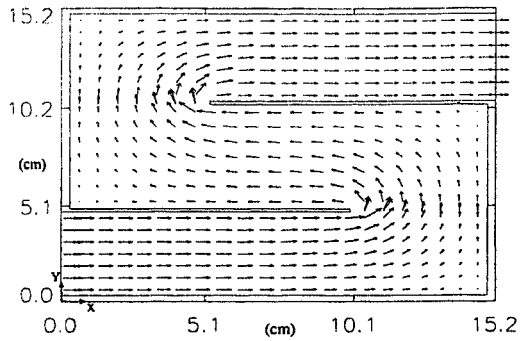

Figure 10: Velocity vectors at centerline (x-y plane) of fin stock (Flow rate = 3.5x10 $^{-3}$ kg/s, Power level = 200 W.)

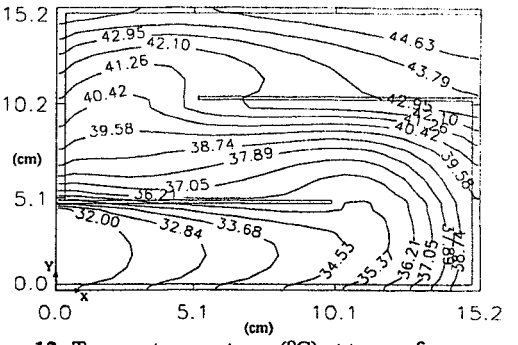

Figure 12: Temperature contours (°C) at top surface (x-y plane) of fin stock (Flow rate = 3.5x10^{-3} kg/s, Power level = 200 W.)

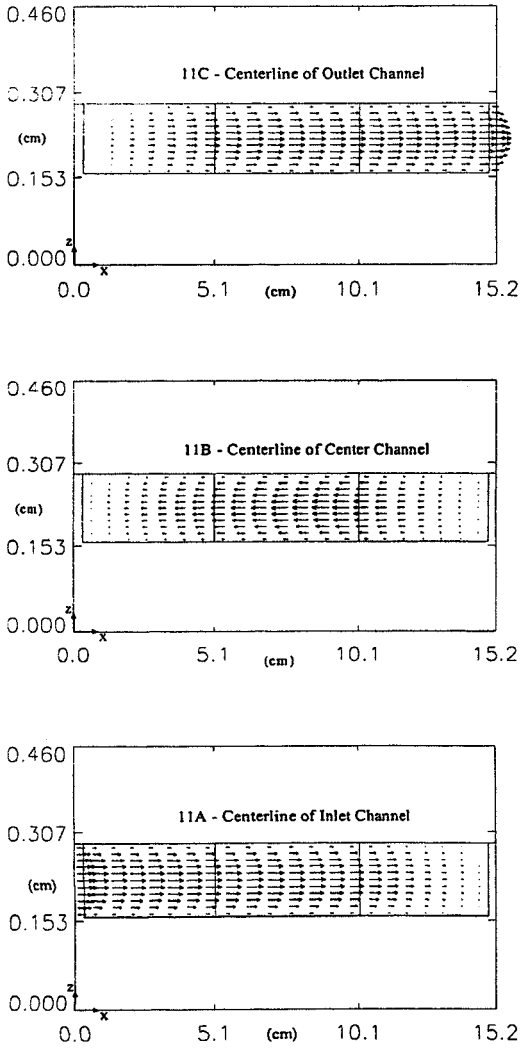

Figure 11: Velocity vectors at centerline (x-z plane) of fin stock in each channel (Flow rate = 3.5x10^{-3} kg/s, Power level = 200 W.)

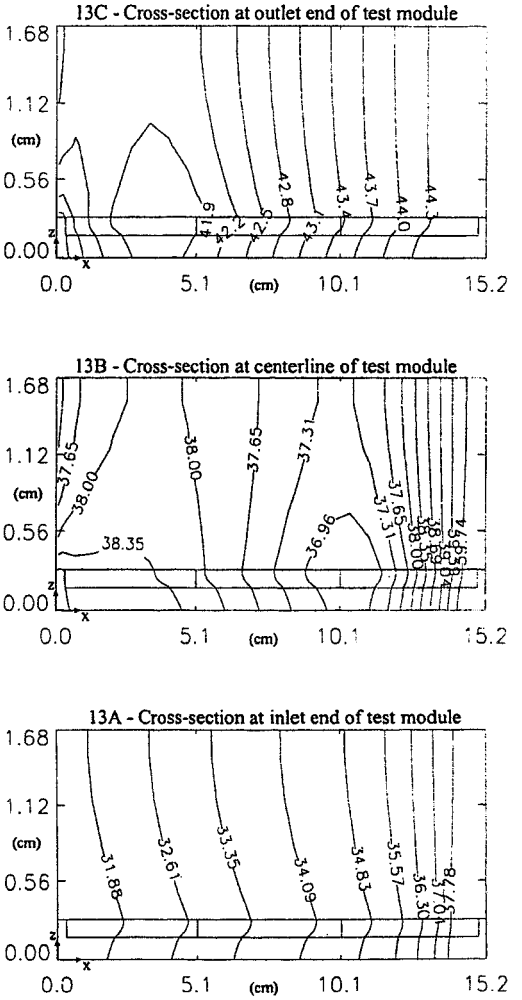

Figure 13: Temperature contours (°C) through cross-section (x-z plane) of test module (Flow rate = 3.5x10^{-3} kg/s, Power level = 200 W.)

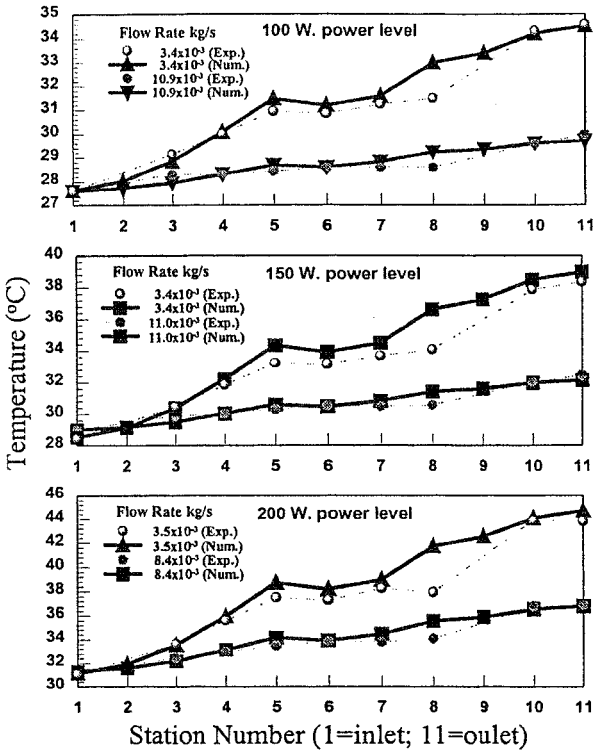

Figure 14: Temperature profile along length of test module (Experimental vs. Numerical)

200 W and $3.5x10^{-3}$ kg/s flow rate are shown in **Figures 10** through **13**. The velocity vectors shown in **Figures 10** and **11** are the Darcy velocities. The results show large velocities to occur at the ends of the inner walls (υ_{max}= 0.13 m/s) while areas of near stagnation occur at the corners. Similar flow patterns were seen during testing by inducing bubbles into the flow, upstream of the test section, and observing their flow path through the channels.

Figures 12 and 13 show the calculated temperature contours within the module. Temperatures for each specific thermocouple location in the test section were also calculated and are plotted against the experimental data in **Figure 14**. The temperature distribution predicted using the porous media model was in generally good agreement with the experimentally obtained temperatures. With the exception of station #8, the model provided a good approximation of the temperature profile, including the plateau effect observed through the middle channel.

Referring back to **Figures 10** and **12** the reason for this plateau becomes clearer. It appears that the relative stagnation in the area to the upper right of station #5 produces a "hot-spot" in that region. Downstream, stations #6 and #7 benefit from an increased local flow rate (and therefore enhanced cooling) which helps them maintain a lower relative temperature

The discrepancy at station #8 may be the result of poor thermal contact between the thermocouple and the fin structure; slight differences in the actual position of the thermocouple verses the assumed location, or some combination of these factors.

It is also interesting to note that aside from station #8, station #5 showed the largest discrepancy between predicted and measured temperature. During testing, station #5's temperature reading showed the largest instability from test to test, sometimes varying by as much as 10% - 20% from the values shown in the figures. In comparison, the other thermocouples (including #8) produced relatively consistent readings between repeated tests. It perhaps is no coincidence then that the model predicts station #5 to be the most sensitive to changes in permeability and positioning due to the large temperature gradient in that area.

V. CONCLUSIONS

A numerical analysis has been presented in which the offset fins of a simulated SEM-E module were modeled as a porous media. Heat transfer results where shown to be in good agreement with experimentally obtained temperatures while qualitative agreement was observed in the calculated flow field. The results of the numerical model were also shown to be only weakly dependent on the permeability used. It may be inferred from this result that the finned array need not be particularly dense to obtain the advantages of having the highly conductive structure within the SEM-E module.

ACKNOWLEDGMENT

This work was supported by a grant from the U.S. Navy Best Manufacturing Practices Program. The authors acknowledge discussions with Mr. Christopher Sims and Mr. Kip Hoffer of the Naval Surface Warfare Center (Crane, Indiana). We are also thankful to Dr. Kai Ho of Brazonics Corporation for providing samples of offset fin structures used in the experiments.

REFERENCES

1. B.V. Antohe, J.L. Lage, D.C. Price, and R.M. Weber, "Thermal Management of High Frequency Electronic Systems with Mechanically Compressed Microporous cold Plates", Proceedings of the 31th National Heat Transfer Conference, ASME HTD vol-329, v7, 1990, pp179-186.

2. J. Bear, *Dynamics of Fluids in Porous Media*, Elsevier, 1972.

3. R. Brinkmann, S. Ramadhayani, T.P. Incropera, "Enhancement of Convective Heat Transfer from Small Heat Sources to Liquid Coolants using Strip Fins", *Experimental Heat Transfer*, v1, 1987, pp315-330.

4. A. Buechler, C.W. Sims, *Liquid-Flow-Through Module/ Cardcage Thermal and Environmental Test Report (NSWC-6043-AECS-5)*, Naval Surface Warfare Center, Crane Division, (1996).

5. Heindel, T.J., Incropera, F.P., Ramadhyani, S., "Enhancement of natural convection heat transfer from an array of discrete heat sources", *International Journal of Heat and Mass Transfer*, v39, n3, 1996, pp479-490.

6. S. Hu, K.E. Herold, "Prandtl Number Effect on Offset Fin Heat Exchanger Performance: Experimental Result", *International Journal of Heat and Mass Transfer*, v38, n6, 1995, pp1053-1061.

7. H.M. Joshi, R.L. Webb, "Heat Transfer and Friction in the Offset Strip Fin Heat Exchanger, *International Journal of Heat and Mass Transfer*, v30, n1, 1987, pp 69-84.

8. M. Kaviany, *Principles of Heat Transfer in Porous Media*, Springer-Verlag, 1991.

9. W.M. Kays, A.L. London, "Heat Transfer and Flow Friction Characteristics of Some Compact Heat Exchanger Surfaces, Part I - Test System and Procedure", *Trans ASME, Journal of Heat Transfer*, v72, 1950, pp 1075-1085.

10. S.J. Kline, "The Purpose of Uncertainty Analysis", Trans. ASME, Journal of Fluids Engineering, v.107, 1985, pp153-164.

11. R.M. Manglik, A.E. Bergles, *Compact Heat Exchangers*, Hemisphere Publishing Corp., 1990, pp 123-148.

12. S.V. Patankar, Numerical Heat Transfer and Fluid Flow, Taylor & Francis, 1980, p131-134.

13. S.V. Patankar, C. Prakash, "An Analysis of the Effects of Plate Thickness on Laminar Flow and Heat Transfer in Interrupted-plate Passages", *International Journal of Heat and Mass Transfer*, v24, n11, 1981, pp1801-1810.

14. E.M. Sparrow, B.R. Baliga, S.V. Patankar, "Heat Transfer and Fluid Flow Analysis of Interrupted-wall Channels with Application to Heat Exchangers, *Trans ASME, Journal of Heat Transfer*, v22, 1977, pp1613-1625.

15. S. Sridhar, Heat Transfer and Pressure Drop in Flows Perpendicular to an Offset fin Structure, *Ph. D. Thesis*, University of Maryland, College Park. (1995)

16. K. Suzuki, E. Haira, T. Sato, T. Mayake, "Numerical and Experimental Studies on a Two-dimensional Model of an Offset-strip Fin Type Compact Heat Exchanger used at Low Reynolds number", *International Journal of Heat and Mass Transfer*, v28, n4, 1985, pp 823-836.

17. A.R. Weiting, "Empirical Correlation for Heat Transfer and Flow Friction Characteristics of Rectangular Offset-fin Plate-fin Heat Exchangers", *Trans ASME, Journal of Heat Transfer*, v97, 1975, pp 488-490.

18. G. Xi, S. Futagami, Y. Hagiwara, K. Suzuki, "Flow and Heat Transfer Characteristics of Offset-fin Array in the Middle Reynolds Number Range", *Proceedings of ASME/JSME Joint Heat Transfer Conference*, v3, 1991, pp 151-156.